Uncertain quantification in nonlinear dynamics with an high-dimensional computational model

Evangéline Capiez-Lernout, Christian Soize

Uncertain quantification in nonlinear dynamics with an high-dimensional computational model

E. Capiez-Lernout [1], **C. Soize** [1]
[1] Université Paris-Est, Laboratoire Modélisation et Simulation Multi-échelle, MSME UMR 8208 CNRS, 5 bd Descartes, 77454 Marne-la-Vallée Cedex 02, France
e-mail: **evangeline.capiez-lernout@u-pem.fr**

Abstract
The present work concerns the dynamical analysis of an uncertain structure in the context of nonlinear dynamics. The structure is assumed to undergo large displacements and large deformations although the constitutive equations remain linearly elastic. The proposed strategy is compatible with the use of high-dimensional computational models, requiring to compute the random dynamical response from a stochastic nonlinear reduced-order model expressed in the time domain. With the proposed method, the uncertainty is introduced by replacing a deterministic chosen reduced-order basis with a stochastic projection basis, for which a new nonparametric probabilistic approach is used so that each realization of the projection basis respects some mathematical properties linked to the available information. The methodology is then applied on a computational model of a bi-clamped tridimensional beam structure.

1 Introduction

A major challenge in many research areas consists in developing advanced methodologies in order to construct predictive numerical simulation tools, which are representative of the observed dynamical behavior dynamical systems. In particular, it is important to quantify how inherent uncertainties propagate on the considered system. Furthermore, an essential aspect is to pay attention to the various nonlinear effects that can subsequently modify the dynamical response of the structure. There have been various researches concerning the development of computational strategies for constructing stochastic nonlinear reduced-order models that are able to accurately reproduce experimental dynamical structural responses that occur in nonlinear vibrational operating ranges. One one hand, a particular attention has to be paid on the construction of nonlinear deterministic reduced-order models [10, 1, 8, 7, 5], that have to be compatible with non intrusive computational strategies regarding existing industrial softwares. On the other hand, uncertainties can be implemented from the mechanical or geometrical parameters of a given deterministic computational model or with nonparametric probabilistic approaches which are parameterized by hyperparameters directly linked to the considered reduced-order models. We are interested in this latter strategy that allows both model and parameter uncertainties to be considered. In previous researches, uncertainty was introduced from the nonlinear reduced-operators issued from a given mean reduced-order model [9, 1, 3]. With the proposed method, the uncertainty is introduced by replacing the deterministic reduced-order basis with a stochastic reduced-order basis. This latter one is obtained by using a new nonparametric probabilistic approach [13, 6] so that each realization of the random projection basis respects some mathematical properties linked to the available information. Moreover, it is parameterized by a small number of hyperparameters. It is then used as the projection basis for constructing the stochastic nonlinear reduced-order model. With such uncertainty modeling, there is no need to construct the stochastic nonlinear reduced operators. The numerical effort is focused on the construction of the stochastic nonlinear reduced internal forces, which is explicitly carried out using the stochastic reduced-order basis combined with the finite element method. The paper is organized

as follows. In Section 2, the computational methodology is described. In particular, the computation of the mean nonlinear dynamical finite element response is used for constructing an adapted reduced-order basis with the proper orthogonal decomposition method. The stochastic nonlinear computational model is then written and the main steps concerning the computational resolution of the set of stochastic nonlinear differential equations are discussed. Section 3 is devoted to a numerical application consisting in a bi-clamped tridimensional beam subjected to a non symmetrical load and for which the uncertainty propagation of the dynamical nonlinear response is analyzed in details.

2 Description of the methodology

2.1 Context of the method

The present research is carried out in the context of the uncertainty propagation for elasto-dynamics structural systems that undergo geometrical nonlinear effects. In this field, a complete methodology has already been developed and a dedicated numerical tool that is adapted for large numerical computational models and that is non intrusive with respect to the industrial softwares has been constructed. More particularly, it has been experimentally validated in the context of the post-buckling of cylindrical shells [2] and applied to various numerical applications [3, 4]. Until now, the uncertainties were modeled through the nonparametric probabilistic approach for which a dedicated probability model issued from the maximum entropy principle [12] was directly implemented on the reduced operators of a mean nonlinear reduced-order model. In particular, such strategy requires the numerical construction of all linear, quadratic, and cubic operators issued from such nonlinear mean reduced-order model. As soon as the probability model is implemented, the numerical construction of the stochastic reduced nonlinear internal forces and of the stochastic tangent operator is then performed. Indeed it is required by the computational algorithms used for solving the stochastic nonlinear differential equations. In the present context, a nonparametric probabilistic approach on the model-form recently introduced in [13] is considered. In this approach, a dedicated probability model of random uncertainties is implemented on the projection basis used for constructing the mean nonlinear reduced-order model. As a consequence, the computational strategy has to be adapted. The main steps of this new methodology are summarized below and the related novel developments are explained in details.

2.2 Mean nonlinear finite element model of the structure

The considered structure is assumed to be fixed on a part of its boundary. In the context of the finite element method, a nonlinear finite element computational model that describes the nonlinear dynamical forced response of the considered structure is characterized in the time domain by the following set of nonlinear coupled differential equations such that

$$[\underline{M}]\ddot{\underline{\mathbf{U}}}(t) + [\underline{D}]\dot{\underline{\mathbf{U}}}(t) + [\underline{K}]\underline{\mathbf{U}}(t) + \underline{\mathbf{F}}^{\mathrm{NL}}(\underline{\mathbf{U}}(t)) = \underline{\mathbf{F}}(t) \quad , \tag{1}$$

$$[\underline{B}]^T \underline{\mathbf{U}}(t) = \mathbf{0} \tag{2}$$

in which the $\mathbb{R}^n$-vector $\underline{\mathbf{U}}(t)$ is the instantaneous displacement vector. In Eq. (1), the real matrices $[\underline{M}]$, $[\underline{D}]$, and $[\underline{K}]$ are the mass and damping, elastic stiffness $(n \times n)$ real matrices with symmetry positive definiteness property. The $\mathbb{R}^n$-vector $\underline{\mathbf{F}}(t)$ is issued from the finite element discretization of the external load and the $\mathbb{R}^n$-vector $\underline{\mathbf{F}}^{\mathrm{NL}}(\underline{\mathbf{U}}(t))$ describes the nonlinear finite element internal forces induced by the geometrical nonlinearities. In Eq. (1), the real $(n \times n_{\mathrm{BC}})$ matrix $[B]$ describes the n_{BC} constraint relations defining the Dirichlet conditions, verifying the relation $[\underline{B}]^T[\underline{B}] = [I_{n_{\mathrm{BC}}}]$. Since we are interested in analyzing the nonlinear vibrations of the structure, the external load is defined in the time domain for $t \in \mathbb{R}$ and a Fourier transform with respect to the time domain is performed on the nonlinear solution and allows then the nonlinear dynamical response in the frequency domain to be analyzed. In the present research, it is chosen to solve this set of nonlinear differential equations in order to construct the nonlinear dynamical response that

will be considered as the reference response. In this case, the nonlinear algorithms require to construct the nonlinear internal finite element forces and the related tangential operator with the finite element model. it should be noted that this calculation is particularly time consuming but is carried out once.

2.3 Construction of the projection basis

The construction of the mean nonlinear reduced-order model requires a projection basis. In the present work, such projection basis is computed from the nonlinear reference response with the proper-orthogonal decomposition method (POD-method), which is proved to be particularly relevant for nonlinear problems. Let $[A]$ be the $(n \times n)$ correlation matrix related to the nonlinear reference dynamical response $\underline{\mathbf{U}}(t)$. It is defined by

$$[\underline{A}] = [\underline{\mathbb{Y}}]^T [\underline{\mathbb{Y}}] \quad , \quad [\underline{\mathbb{Y}}]_{ij} = \underline{U}_i(t_j) \sqrt{\delta t} \quad , \tag{3}$$

in which δt is the constant sampling time step, and where t_j denotes the sampling time number j. The projection basis is defined by the eigenvectors $\underline{\boldsymbol{\varphi}}_\alpha$ related to the N most contributing eigenvalues $\underline{\lambda}_\alpha$, solution of

$$[\underline{A}]\, \underline{\boldsymbol{\varphi}}_\alpha = \underline{\lambda}_\alpha\, \boldsymbol{\varphi}_\alpha \quad \text{with} \quad \underline{\boldsymbol{\varphi}}_\alpha^T\, \underline{\boldsymbol{\varphi}}_\beta = \delta_{\alpha\beta} \quad , \tag{4}$$

in which $\delta_{\alpha\beta}$ is the Kronecker symbol set to 1 if $\alpha = \beta$ and to 0 otherwise. Note that in practice, for large computational models, the numerical construction of correlation matrix $[A]$ is difficult to achieve. In such a case, metrics $[A]$ is not computed and the eigenvalue problem is replaced by a singular value decomposition of metrics $[Y]$ or $[Y]^T$ (see Section 3.3).

2.4 Stochastic nonlinear reduced-order model

In this work, the nonparametric probabilistic approach of model-form uncertainties recently introduced in [13] is used. In such case, the probability model is directly implemented in the projection basis. Let $[\underline{\Phi}]$ be the $(n \times N)$ matrix whose columns are the eigenvectors $\underline{\boldsymbol{\varphi}}_1, \cdots, \underline{\boldsymbol{\varphi}}_N$. The matrix $[\underline{\Phi}]$ is then replaced by a stochastic matrix $[\boldsymbol{\Phi}(\boldsymbol{\alpha})]$, whose stochastic model and whose Monte Carlo numerical simulation procedure is found in [13]. It should be noted that the random vectors contained in random matrix $[\boldsymbol{\Phi}]$ verify the boundary conditions and orthonormality conditions

$$[\underline{B}]^T [\boldsymbol{\Phi}] = \mathbf{0} \quad , \quad [\boldsymbol{\Phi}]^T [\boldsymbol{\Phi}] = [I_N] \quad , \tag{5}$$

in which $[I_N]$ is the identity matrix with N order. The probability distribution of random matrix $[\boldsymbol{\Phi}]$ depends on a $\mathbb{R}^m$-valued hyperparameter $\boldsymbol{\alpha} = \{s, \beta, [\sigma]\}$, with $m = 0.5N(N+1)+2$. More specifically, s is a scalar which controls the global amount of uncertainty on the random basis, β is a scalar which controls the noise level around each projection vector basis and $[\sigma]$ is an $(N \times N)$ real upper triangular matrix which allows the correlations between the projection basis vectors to be controlled.

The stochastic computational model consists then in solving the set of stochastic nonlinear differential equations

$$[\boldsymbol{\mathcal{M}}] \ddot{\mathbf{Q}}(t) + [\boldsymbol{\mathcal{D}}] \dot{\mathbf{Q}}(t) + [\boldsymbol{\mathcal{K}}] \mathbf{Q}(t) + [\boldsymbol{\Phi}]^T \underline{\mathbf{F}}^{\mathrm{NL}}([\boldsymbol{\Phi}]\, \mathbf{Q}(t)) = [\boldsymbol{\Phi}]^T \underline{\mathbf{F}}(t) \quad , \tag{6}$$

in which $[\boldsymbol{\mathcal{M}}] = [\boldsymbol{\Phi}]^T\, [\underline{M}]\, [\boldsymbol{\Phi}]$, $[\boldsymbol{\mathcal{D}}] = [\boldsymbol{\Phi}]^T\, [\underline{D}]\, [\boldsymbol{\Phi}]$ and $[\boldsymbol{\mathcal{K}}] = [\boldsymbol{\Phi}]^T\, [\underline{K}]\, [\boldsymbol{\Phi}]$ are the full random mass, damping and stiffness matrices belonging to the set of positive-definite symmetric $(N \times N)$ real-valued matrices, and where $\mathbf{Q}$ is the $\mathbb{R}^N$-valued random vector of the generalized coordinates from which the $\mathbb{R}^n$-valued random vector of the physical solution $\mathbf{U}$ is reconstructed by

$$\mathbf{U} = [\boldsymbol{\Phi}]\, \mathbf{Q} \quad . \tag{7}$$

Regarding the numerical computation, the set of these stochastic nonlinear differential equations is solved in the time domain by using the Monte Carlo numerical simulation, using an implicit and unconditionally

stable integration scheme (Newmark method with the averaging acceleration scheme). For each sampling time, the nonlinearity is solved iteratively by using either the fixed point method or an arc-length-based algorithm, depending on the nonlinearity rate. Concerning the current strategy, the knowledge of the nonlinear reduced-order internal force vector is required by both nonlinear algorithms whereas the knowledge of the related reduced tangent operator (that is time consuming) is only required by the use of the arc-length-based algorithm. Practically, the contributions of both nonlinear reduced-order internal force and tangent reduced operator induced by each finite element are explicitly constructed with the finite element method. The assemblage over the finite elements is particularly quick because it only requires to sum each of these contributions. A posterior nonlinear dynamical analysis is performed from Eq.(7) in the frequency domain by computing the Fourier transform of the nonlinear dynamical response.

3 Numerical application

3.1 Description of the finite element computational model

The three-dimensional bounded domain Ω is a slender rectangular domain defined in a Cartesian system $(0, \mathbf{e}_1, \mathbf{e}_2, \mathbf{e}_3)$ such that $\Omega =]0, \underline{l}[\times]0, \underline{b}[\times]0, \underline{h}[$ with $\underline{l} = 8\,m$, $\underline{b} = 0.8\,m$, $\underline{h} = 0.6\,m$. Let Γ_0 and Γ_1 be the boundaries described as $\Gamma_0 = \{\mathbf{x};\, x_1 = 0\}$ and $\Gamma_1 = \{\mathbf{x};\, x_1 = \underline{l}\}$. The structure is assumed to be fixed on both boundaries so that we have a Dirichlet condition on $\Gamma_0 \bigcup \Gamma_1$. The structure is free on boundary $\partial\Omega \setminus \{\Gamma_0 \bigcup \Gamma_1\}$. The structure is subjected to an external point load applied along directions $\mathbf{e}_1$, $\mathbf{e}_2$ and $\mathbf{e}_3$ at the excitation node located at $(3.2, 0.4, 0.6)$. The Young modulus, the Poisson coefficient and the mass density of the homogeneous and isotropic linear elastic material are $\underline{E} = 2 \times 10^{11}\, N.m^{-2}$, $\underline{\nu} = 0.3$ and $\underline{\rho} = 8200\, Kg.m^{-3}$. A three dimensional finite element model is constructed with $40 \times 4 \times 3 = 480$ solid finite elements with 8 nodes. Therefore, the mean computational model has 820 nodes and $n = 2\,320$ degrees of freedom (see Fig. 1).

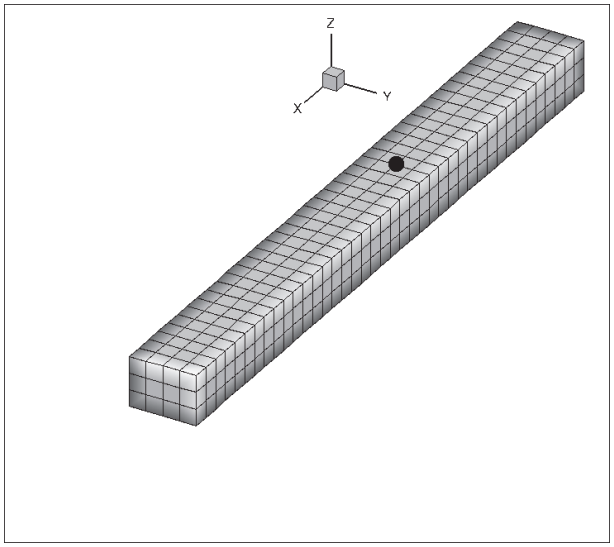

Figure 1: Finite element mesh of the structure - localisation of the excitation node (• symbol).

It should be noted that the fundamental eigenfrequency related to the linear undamped structure is $\nu_1 = 47.930\, Hz$. The frequency band of analysis is then chosen as $\mathbb{B} = [40\,,\, 2000]\, Hz$. The damping is then represented by a Rayleigh model $[D] = \alpha\,[M] + \beta\,[K]$ with $\alpha = 24.2$ and $\beta = 9.4 \times 10^{-6}$, which corresponds to a critical damping rate $\xi_1 = 0.040$ at fundamental frequency ν_1 and such that $\xi \in [0.015, 0.060]$ in frequency band $\mathbb{B}$. The chosen observation node is located at $(3.2, 0.4, 0.6)$, where the external point load is applied.

3.2 Description of the external loading

We are interested in analyzing the nonlinear dynamical forced response in frequency band $\mathbb{B}$. The chosen excitation frequency band is $\mathbb{B}_{exc} = [450\,,\,1200]\,Hz$. The load intensity is chosen as $f_0 = 18 \times 10^6\,N$ that corresponds to a consequent rate of geometrical nonlinearity for the numerical application presented. Consequently, it is no longer possible to directly compute the forced response in the frequency domain. The forced response is then computed in the time domain according to Eq.(1) and Eq. (2). The time dependent function $g(t)$ is defined with $\Delta\nu = 750\,Hz$ and $s = 1.1$. Practically, the computation is carried on a truncated time domain $\mathbb{T} = [t_{ini}, t_{ini} + T]$. The initial load is chosen as $t_{ini} = -4/\Delta\nu = -0.053\,s$ yielding a null initial load. The time duration T is then adjusted so that the system be returned at its equilibrium state within a given numerical tolerance for both linear and nonlinear computations. Even the fundamental eigenfrequency does not belong to excitation frequency band $\mathbb{B}_{exc}$, it ca be indirectly excited through the geometrical nonlinear effects. Time duration is chosen as $T = 0.234\,s$ which ensures the system to return to its equilibrium state with a relative tolerance $\tau = e^{-2\pi\xi_1\nu_1 T} = 6\%$ when fundamental eigenfrequency is excited. The sample frequency ν_e and the number of time steps are then chosen as $\nu_e = 35\,000\,Hz$ and $n_t = 8\,192$ yielding a constant sampling time step $\delta t = 2.857 \times 10^{-5}\,s$ and a constant sampling frequency step $\delta\nu = 4.272\,Hz$. It should be noted that the fundamental resonance that could possibly be excited would be nearly correctly represented with such computational choice. Let $t_\alpha = t_{ini} + \alpha\delta t\,, \alpha \in \{0, \cdots, n_t - 1\}$ and let $\nu_\beta = -0.5\nu_e + \beta\delta\nu\,, \beta \in \{0, \cdots, n_t - 1\}$. The Fourier transform $\widehat{g}(2\pi\nu)$ of function $g(t)$ is numerically estimated by using the Fast Fourier Transform since function $\widehat{g}(2\pi\nu)$ can be written as

$$\widehat{g}(2\pi\nu_\beta) = \exp\left(i\pi\, t_{ini}\nu_e\right)\, \exp\left(2i\pi\beta\delta\nu t_{ini}\right) \sum_{\alpha=0}^{n_t-1} (-1)^\alpha\, g(t_\alpha)\, exp(-2i\pi\alpha\beta/n_t) \quad . \tag{8}$$

Figure 2 displays the graphs of function $t \mapsto g(t)$ and $\nu \mapsto |\widehat{g}(2\pi\nu)|$.

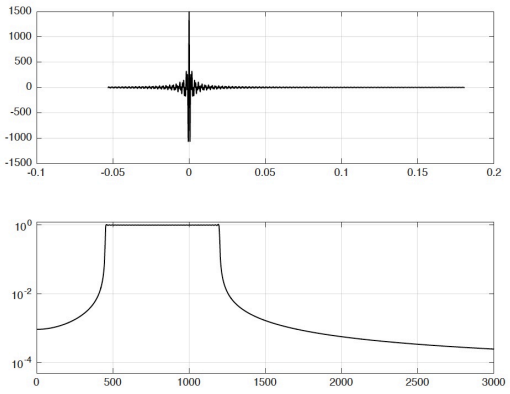

Figure 2: Representation of the time dependent load in the time domain and in the frequency domain : graphs of $t \mapsto g(t)$ (upper graph) and $\nu \mapsto |\hat{g}(2\pi\nu)|$ (lower graph).

3.3 Construction of the projection basis for the mean nonlinear reduced-order model

The dynamical response of the mean nonlinear finite element model is first calculated according to the algorithm described in Section 2.4. Figure 3 displays the graphs of both linear and nonlinear finite element dynamical responses at the observation node along the three dimensions in the time domain. It can be seen that the chosen load intensity yields subsequent geometrical nonlinear effects. Indeed, it can be seen that the dynamical response amplitudes are limited by the geometrical nonlinear effects. Moreover, the dynamical

system returns to its equilibrium state with a longer delay, in particular for the transverse directions. This means that the resonances that are located outside and below the excitation frequency band are indirectly excited by the geometrical nonlinearities. In order to quantify such geometrical nonlinear effects, a Fourier transform of both nonlinear and linear responses is carried out in the frequency domain. Figure 4 displays the graph of the response amplitude related to the observation node in the frequency domain for both nonlinear and linear cases. It is clearly seen that there exists a consequent contribution of resonances located in the very low frequency band outside the excitation frequency band.

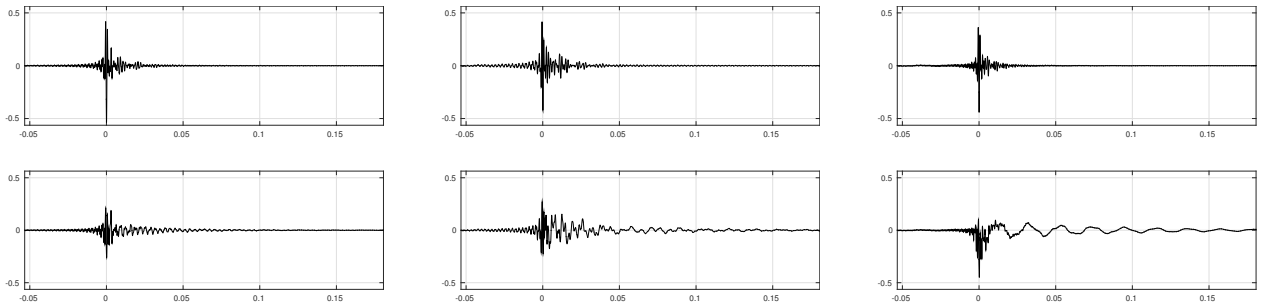

Figure 3: Time domain observation $t \mapsto u_{obs,1}(t)$ (left figure), $t \mapsto u_{obs,2}(t)$ (middle figure), $t \mapsto u_{obs,3}(t)$ (right graph) related to the linear (upper graph) and to the nonlinear (lower graph) finite element dynamical responses.

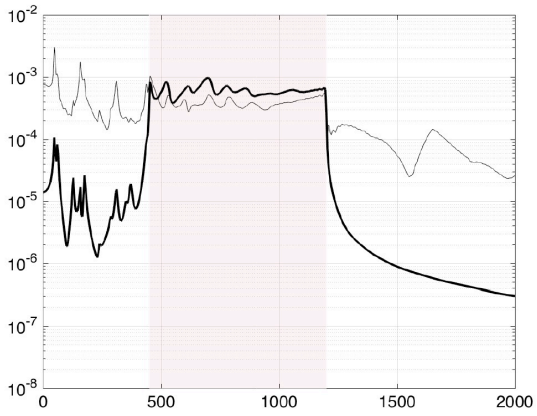

Figure 4: Frequency domain observation $\nu \mapsto ||\widehat{u}_{obs}(2\pi\nu)||$ related to the linear (thin black line) and to the nonlinear (thick black line) finite element dynamical responses for excitation frequency band $\mathbb{B}_{exc} = [450\ ,\ 1200]\, Hz$ (light red zone).

The mean nonlinear finite element dynamical response is then used for constructing the projection basis with the POD-method as described in Section 2.4. Practically, in the present case, since $n < n_t$, the projection basis is numerically calculated by using the single value decomposition of matrix $[\mathbb{Y}]^T$ whose singular values s_α are sorted by decreasing order and such tha $s_\alpha^2 = \lambda_\alpha$ and whose right-singular vectors corresponds to the basis vectors $\boldsymbol{\varphi}_\alpha$. Note that the projection basis strongly depends on the nature of the external load, which requires to be computed for each considered load case. Figure 5 displays several basis vectors issued from this POD decomposition. It is clearly seen that this projection basis presents local spatial displacements around the excitation node (that was expected), contrarily to a usual basis constituted of linear elastic eigenmodes.

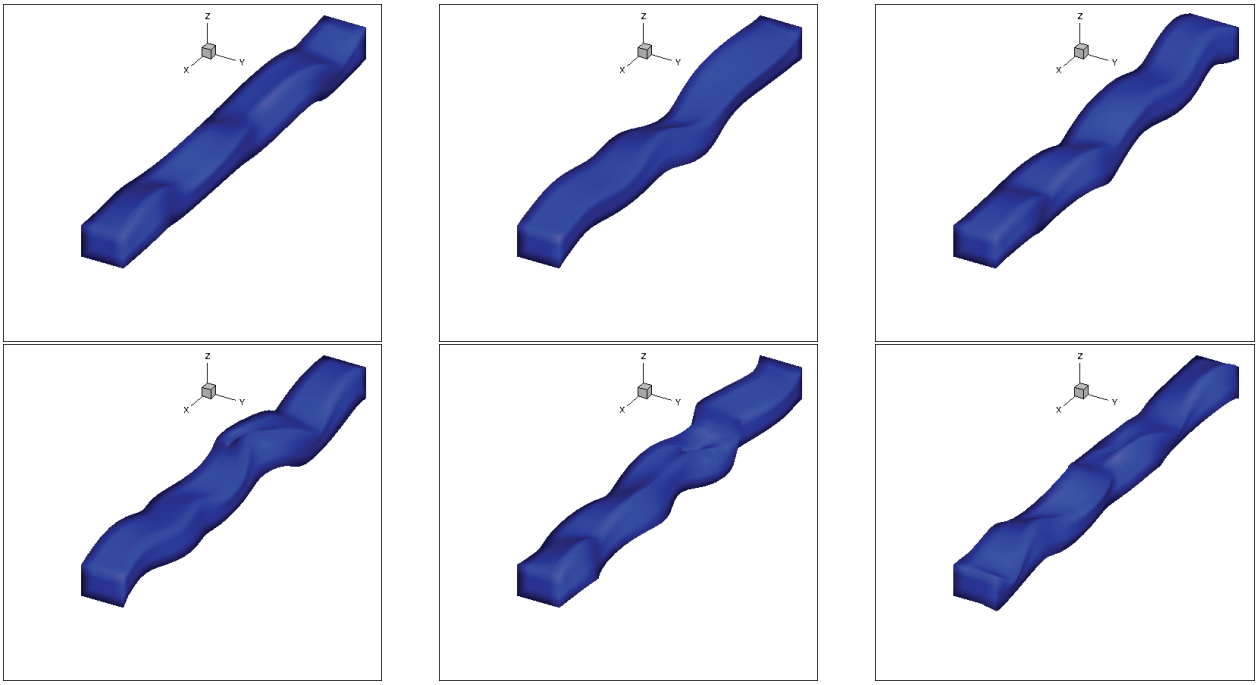

Figure 5: Representation of several basis vectors belonging to the projection basis computed with the POD method over the mean nonlinear finite element dynamical response.

3.4 Computational validation of the mean nonlinear reduced-order model

First a convergence analysis is performed in order to set the optimal order of the mean nonlinear reduced-order model that can accurately reproduce the nonlinear finite element response. Let $N \mapsto Conv_s(N)$ and $N \mapsto Conv_Q(N)$ be the convergence functions defined by

$$Conv_s(N) = \sqrt{\frac{\sum_{\alpha=1}^{N} s_\alpha^2}{\sum_{\alpha=1}^{n} s_\alpha^2}} \tag{9}$$

$$Conv_Q(N) = \sqrt{\frac{\int_0^{+\infty} ||\widehat{\mathbf{Q}}^N(2\pi\nu)||^2 \, d\nu}{\int_0^{+\infty} ||\widehat{\mathbf{U}}^{ref}(2\pi\nu)||^2 \, d\nu}} \quad . \tag{10}$$

Figure 6 displays the graph of function $N \mapsto Conv_s(N)$. Since the projection basis is orthonormal, it can easily be shown that $Conv_Q(n) = 1$. Figure 7 displays the graph of function $N \mapsto Conv_Q(N)$. It is seen that a good agreement is obtained for $N = 60$. From now on, we use $N = 60$ in the numerical application. In previous researches, the chosen projection basis was issued from nonlinear static calculations or from linear elastic modes which did not require the knowledge of the mean nonlinear finite element dynamical response. As a consequence, the systematic convergence analysis carried out with the mean nonlinear reduced-order model was converging towards a certain value yielding a converged value of N. But there was no computational proof that such converged value was the good one. In the present strategy, a computational effort for solving the mean nonlinear finite element model has been carried out. Consequently, it is computationally proved that the converged nonlinear dynamical response obtained with the mean nonlinear reduced-order model corresponds to the reference nonlinear finite element dynamical response.

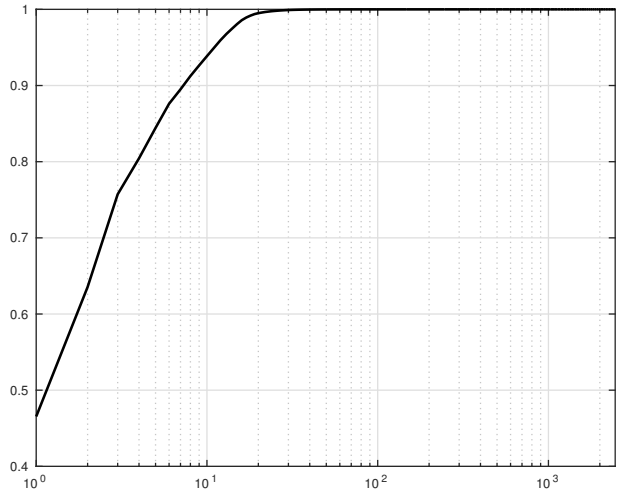

Figure 6: Convergence analysis for the mean nonlinear reduced-order model : graph of function $N \mapsto Conv_s(N)$.

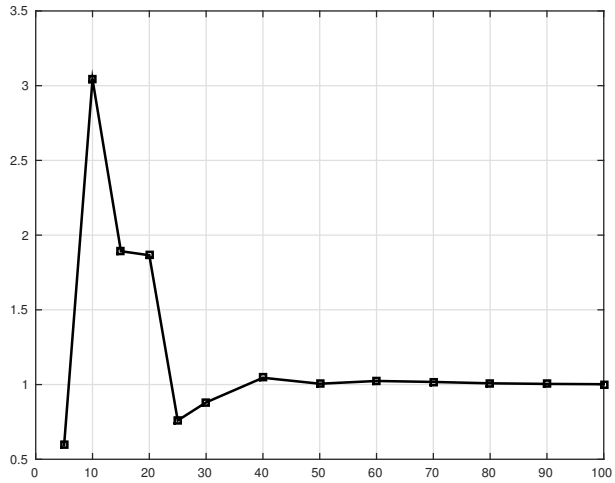

Figure 7: Convergence analysis for the mean nonlinear reduced-order model : graph of function $N \mapsto Conv_Q(N)$.

3.5 Stochastic nonlinear dynamical response

This Section is devoted to the stochastic nonlinear dynamical analysis of the structure. The computational results are presented for $s=0.003$, $\beta=0.0025$ and $[\sigma]$ an upper triangular matrix with N order for which the non-zeros entries are defined by $[\sigma]_{ii} = 10$, $[\sigma]_{i,i+1} = 5$ and $[\sigma]_{i,i+2} = 2.5$. The results are computed with $n_s=70$ Monte Carlo numerical realizations.

An experimental data basis is assumed to be available for the three observation dofs. Such experimental response is computed numerically as follows : The material properties $\underline{E}$, $\underline{\nu}$, $\underline{\rho}$ are replaced by stochastic fields $\mathbf{E}(\mathbf{x})$, $\boldsymbol{\nu}(\mathbf{x})$ and $\boldsymbol{\varrho}(\mathbf{x})$ yielding inhomogeneous materials along the length of the beam and we have then

$$\begin{aligned} \mathbf{E}(\mathbf{x}) &= \underline{E}(1+0.03\sum_{i=0}^{I} \boldsymbol{\xi}_i \sin\left(\frac{0.02\pi i}{\underline{\ell}}(x-0.5\underline{\ell})\right) \quad , \\ \boldsymbol{\nu}(\mathbf{x}) &= \underline{\nu}(1+0.03\sum_{i=0}^{I} \boldsymbol{\xi}'_i \sin\left(\frac{0.02\pi i}{\underline{\ell}}(x-0.5\underline{\ell})\right) \quad , \end{aligned} \tag{11}$$

$$\mathfrak{g}(\mathbf{x}) \quad = \quad \underline{\rho}(1+0.03\sum_{i=0}^{I}\boldsymbol{\xi}_i''\sin\left(\frac{0.02\pi i}{\underline{\ell}}(x-0.5\underline{\ell})\right) \quad ,$$

in which $\boldsymbol{\xi}_i$, $\boldsymbol{\xi}_i'$ and $\boldsymbol{\xi}_i''$ are independent truncated Gaussian random variables in order that $\forall \mathbf{x} \in \Omega$, $\mathbf{E}(\mathbf{x}) > 0$, $\boldsymbol{\nu}(\mathbf{x}) \in]0\,,1/2[$ and $\mathfrak{g}(\mathbf{x}) > 0$ almost surely. Note that the nonlinear stochastic computational model cannot reproduce this experimental data.

Let $\mathbf{u}_{exp}(2\pi\nu)$ be the vector of the experimental response. Figures 8 , 9 and 10 display the graph of function $\nu \mapsto |\mathbf{u}_{obs,i}(2\pi\nu)|$ (black dashed line), $\nu \mapsto |\mathbf{u}_{exp,i}(2\pi\nu)|$ (red line), and the graph of the confidence region of random function $\nu \mapsto |\mathbf{U}_{obs,i}(2\pi\nu)|$ of the observation with a probability level $p_c = 0.95$ related to the nonlinear reduced-order model for $i \in \{1,2,3\}$. First, it can be seen that unexpected resonances that are induced by the geometrical nonlinear effects and that are located in the low frequencies outside $\mathbb{B}_{exc}$ appear with subsequent amplitudes. Concerning the longitudinal displacement, it is seen that the proposed computational model captures well the nonlinear experimental dynamical behavior. Concerning the transverse displacements, we have a good agreement between the computational model and the experimental response except for the first resonance. It should be noted that the presented results have been obtained for a selected value of $\boldsymbol{\alpha}$, which does not correspond to an optimal value that would be obtained by solving an optimization problem allowing for minimizing the distance to the experimental target.

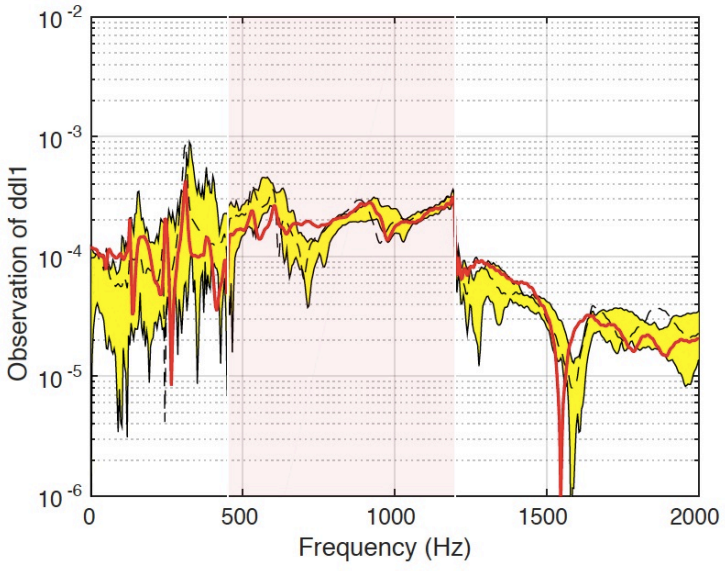

Figure 8: Graph of functions $\nu \mapsto |\mathbf{u}_{obs,1}(2\pi\nu)|$ (black dashed line) computed with the nonlinear finite element model, $\nu \mapsto |\mathbf{u}_{exp,1}(2\pi\nu)|$ (red line), graph of the confidence region of random function $\nu \mapsto |\mathbf{U}_{obs,1}(2\pi\nu)|$ computed with the nonlinear stochastic reduced-order model (yellow zone), localization of the excitation frequency band $\mathbb{B}_{exc} = [450\,,\,1200]\,Hz$ (light red zone).

4 Conclusion

In the context of structural dynamics with geometric nonlinearities, a computational methodology is presented for analyzing the propagation of uncertainties on the nonlinear dynamical response. A nonparametric probabilistic method for modeling model-form uncertainties, which is implemented from a given projection basis is used for constructing a stochastic computational nonlinear reduced-order model . A numerical application, which consists in a bi-clamped beam, is presented and shows the capability of the stochastic computational model to capture the unexpected resonances induced by the geometrical nonlinearities.

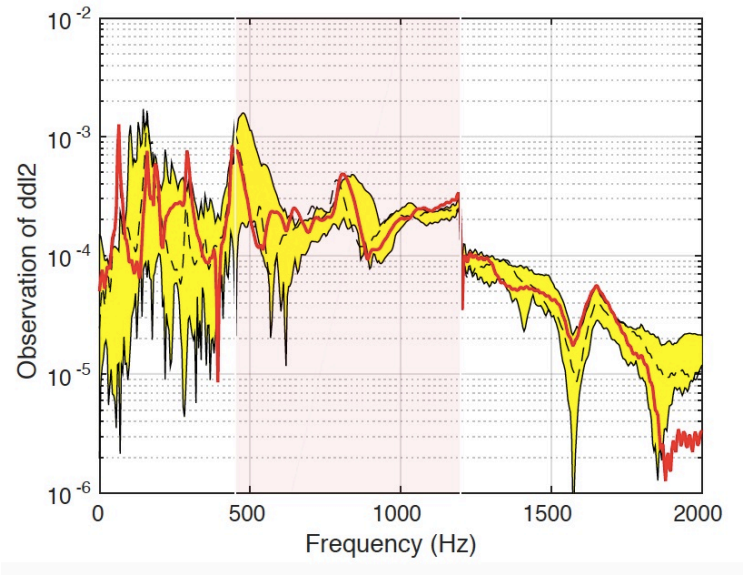

Figure 9: Graph of functions $\nu \mapsto |\mathbf{u}_{obs,2}(2\pi\nu)|$ (black dashed line) computed with the nonlinear finite element model, $\nu \mapsto |\mathbf{u}_{exp,2}(2\pi\nu)|$ (red line), graph of the confidence region of random function $\nu \mapsto |\mathbf{U}_{obs,2}(2\pi\nu)|$ computed with the nonlinear stochastic reduced-order model (yellow zone), localization of the excitation frequency band $\mathbb{B}_{exc} = [450\ ,\ 1200]\ Hz$ (light red zone).

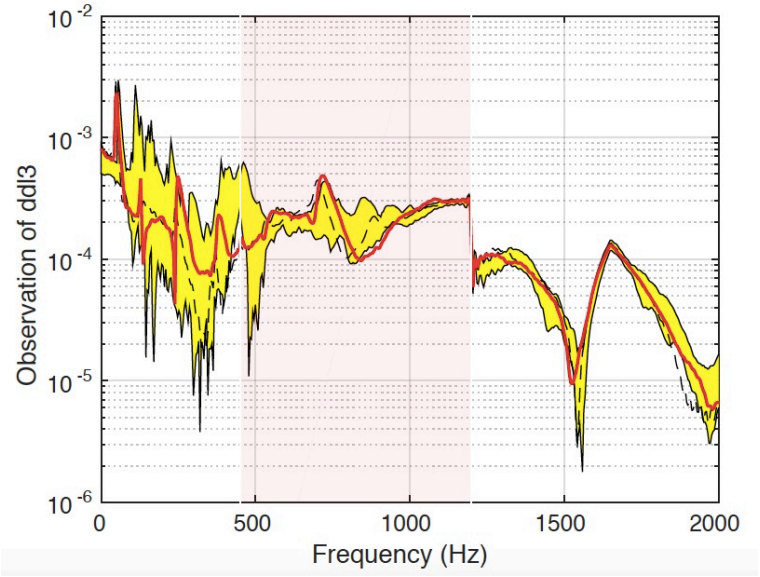

Figure 10: Graph of functions $\nu \mapsto |\mathbf{u}_{obs,3}(2\pi\nu)|$ (black dashed line) computed with the nonlinear finite element model, $\nu \mapsto |\mathbf{u}_{exp,3}(2\pi\nu)|$ (red line), graph of the confidence region of random function $\nu \mapsto |\mathbf{U}_{obs,3}(2\pi\nu)|$ computed with the nonlinear stochastic reduced-order model (yellow zone), localization of the excitation frequency band $\mathbb{B}_{exc} = [450\ ,\ 1200]\ Hz$ (light red zone).

References

[1] E. Capiez-Lernout, C. Soize, M.-P. Mignolet, Computational stochastic statics of an uncertain curved structure with geometrical nonlinearity in three-dimensional elasticity, *Computational Mechanics*, **49**

(1) 87-97 (2012).

[2] E. Capiez-Lernout, C.Soize, M.-P.Mignolet, Post-buckling nonlinear static and dynamical analyses of uncertain cylindrical shells and experimental validation, *Computer Methods in Applied Mechanics and Engineering*, **271**, 210-230 (2014).

[3] E. Capiez-Lernout, C. Soize, and M. Mbaye. Mistuning analysis and uncertainty quantification of an industrial bladed disk with geometrical nonlinearity. *Journal of Sound and Vibration*, 356(11):124–143, 2015.

[4] E. Capiez-Lernout and C. Soize. An improvement of the uncertainty quantification in computational structural dynamics with nonlinear geometrical effects. *International journal for Uncertainty Quantification*, 7(1):83–98, 2017.

[5] C. Farhat, P. Avery, T. Chapman and J. Cortial. Dimensional reduction of nonlinear finite element dynamic models with finite rotations and energy-based mesh sampling and weighting for computational efficiency. *International Journal for Numerical Methods in Engineering*, 98(9):625-662, 2014.

[6] C. Farhat, A. Bos, P. Avery and C. Soize. Modeling and quantification of model-form uncertainties in eigenvalue computations using a stochastic reduced model. *AIAA Journal*, 56(3):1198–1210,2018.

[7] A.K. Gaonkar and S.S. Kulkami. Model order reduction for dynamic simulation of beams with forcing and geometric nonlinearities *Finite Elements in Analysis and Design*, 76:50-62, 2013.

[8] M.-P. Mignolet, A. Przekop, S.A. Rizzi, and M.S. Spottswood. A review of indirect/non-intrusive reduced-order modeling of nonlinear geometric structures. *Journal of Sound and Vibration*, 332(10):2437–2460, 2013.

[9] M.-P. Mignolet and C. Soize. Stochastic reduced-order models for uncertain geometrically nonlinear dynamical systems. *Computer Methods in Applied Mechanics and Engineering*, 197:3951–3963, 2008.

[10] A.A. Muryavov and S.A. Rizzi. Determination of nonlinear stiffness with application to random vibration of geometrically nonlinear structures. *Computers and Structures*, 81:1513–1523, 2003.

[11] L. Sirovich. Turbulence and the dynamics of coherent structures *Quarterly of Applied Mathematics*, 45(3):561–571, 1987.

[12] C. Soize. *Stochastic Models of Uncertainties in Computational Mechanics*. Lecture Notes in Engineering Mechanics 2, American Society of Civil Engineers (ASCE), 2012.

[13] C. Soize and C. Farhat. A nonparametric probabiistic approach for quantifying uncertainties in low-dimensional and high-dimensional nonlinear models. *International Journal for Numerical Methods in Engineering*, 109(6):837-888, 2017.